Journal of Materials Chemistry

www.rsc.org/materials

Volume 20 | Number 17 | 7 May 2010 | Pages 3321 - 3516

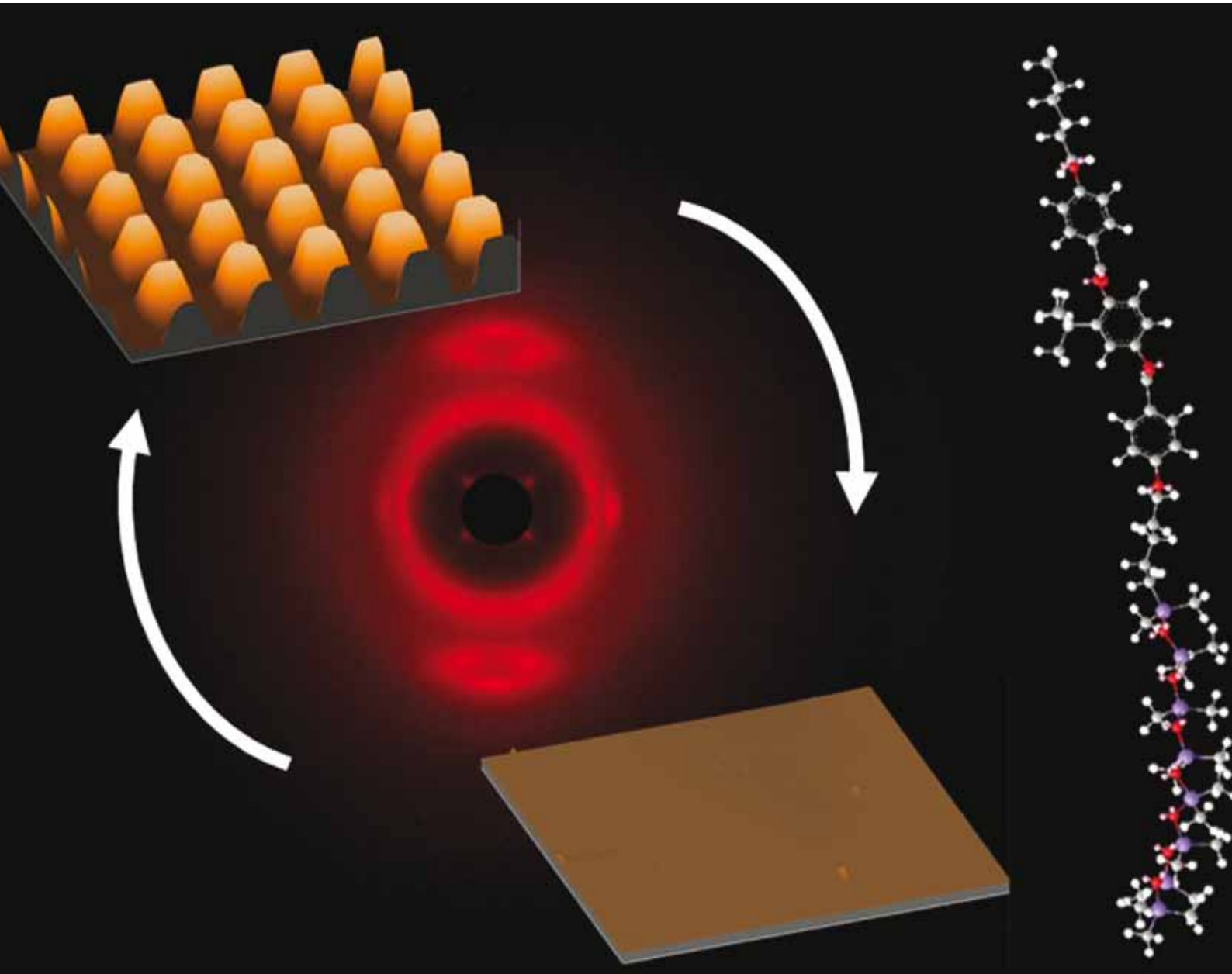

Actively Moving Polymers

ISSN 0959-9428

RSC Publishing

0959-9428(2010)20:17;1-N

Soft shape memory in main-chain liquid crystalline elastomers†‡

Kelly A. Burke[ab] **and Patrick T. Mather***[bc]

Received 16th November 2009, Accepted 15th January 2010
First published as an Advance Article on the web 15th February 2010
DOI: 10.1039/b924050k

The field of shape memory polymers (SMPs) has been dominated by polymeric network systems whose fixing mechanism is based on crystallization or vitrification of the constituent chains, rendering such systems stiff in comparison to elastomers, gels, and living tissues. In this report, we describe the synthesis and characterization of liquid crystalline elastomers that exhibit both bulk and surface shape memory effects with compositionally dependent transition temperatures that determine the shape fixing and shape recovery critical temperatures. Main-chain, segmented liquid crystalline elastomers were synthesized using hydrosilylation linking of poly(dimethylsiloxane) oligomers with mesogenic dienes of two compositions and a tetrafunctional crosslinker. Calorimetric and dynamic mechanical analyses revealed two composition-determined thermal transitions for the LCEs, including a glass transition event at low temperatures (33 °C < T_g < 48 °C) and a first-order isotropization transition at higher temperatures (57 °C < T_i < 71 °C), each increasing with an increase in the concentration of the more slender, unsubstituted mesogenic diene, ***5H***. Despite the existence of a glass transition event, the materials remain soft at low temperature, a finding explained by vitrification of only the mesogen-rich layers within the smectic phase. Shape memory behavior was evaluated quantitatively and revealed excellent shape fixing and shape recovery values, generally in excess of 98%, with the recovery temperature depending on composition in a manner determined by the LCE phase behavior, particularly T_g. The temperature-dependent kinetics of shape memory were analyzed for a selected LCE composition, revealing exponential time dependence with rate constants that depended on temperature in an Arrhenius manner. Finally, the softness of the LCE SMPs was exploited to fix an embossed, micron-scale pattern on the surface and then recover the equilibrium flat state quite completely. We envision application of this surface shape memory phenomenon in the areas of soft lithography, especially microcontact printing and microfluidics.

Introduction

Shape memory polymers (SMPs)[1–3] are a class of active materials that are able to "fix" a temporary shape and then later recover to a "memorized" permanent shape established by a covalent or physical network by thermal, electrical, or other environmental stimulus. In many cases, shape memory polymers are characterized by deforming at a temperature above a softening transition, such as the glass transition temperature, T_g, or the melting point, T_m, of the polymer, then cooling through this transition under stress, causing immobilization of the constituent network chains and the macroscopic shape to be "fixed." Recovery of the permanent shape is then accomplished by heating above the triggering temperature, which re-mobilizes the network chains and allows rubber (entropic) elasticity to return the sample to its equilibrium shape.

Many examples of SMPs can be found in the literature, and these may be broadly classified into four classes, defined by their architectural means to achieve shape fixing and recovery, following the convention of Liu *et al.*[2] Class I materials are covalently crosslinked glassy thermoset networks whose triggering temperature is T_g, while class II materials are covalently crosslinked semicrystalline networks whose melting and crystallization allow recovery and fixing, respectively. In both class I and class II materials, the covalent crosslinks engender large-strain elasticity above the triggering temperature. In class III and class IV SMPs, physical crosslinks provide elasticity above the triggering temperature. Class III materials are physically crosslinked glassy blends or multiblock copolymers, where the component or phase with the lower T_g is used as the triggering phase and the component with the higher T_g or T_m serves as the crosslinker and allows for reprocessing of the material. Finally, class IV materials are physically crosslinked semicrystalline block copolymers, where the block that melts at the higher

[a]*Department of Macromolecular Science and Engineering, Case Western Reserve University, 2100 Adelbert Road, Cleveland, OH, 44106, USA*
[b]*Syracuse Biomaterials Institute, Syracuse University, 121 Link Hall, Syracuse, NY, 13244, USA. E-mail: ptmather@syr.edu*
[c]*Department of Biomedical and Chemical Engineering, Syracuse University, 121 Link Hall, Syracuse, NY, 13244, USA*

† This paper is part of a *Journal of Materials Chemistry* themed issue on Actively Moving Polymers. Guest editor: Andreas Lendlein

‡ Electronic supplementary information (ESI) available: (1) Wide-angle X-ray scattering patterns of oriented LCEs are shown to assist in identification of the smectic-C phase. (2) Differential scanning calorimetry of **E-*5H*$_{80}$*5t*B_{20}** annealed for 1 h at 50 °C plotted on expanded temperature and heat flow axes. (3) Selected isothermal strain-recovery experiments with regression fits from the stepped recovery of **E-*5H*$_{80}$*5t*B_{20}**. (4) Selected WAXS patterns and mesogen tilt angle data from a microstructure study of deformed **E-*5H*$_{80}$*5t*B_{20}** (strain initially 194%) recovered by increasing temperature in a stepwise manner. See DOI: 10.1039/b924050k

temperature acts as a crosslinker and the lower melting block is the triggering phase.

When a SMP is deformed and cooled through its triggering temperature, the mechanical work that had been done is stored in the deformed polymeric network chains. Recovery of the elastic entropy of the chains is usually suspended (fixed) by vitrification or crystallization of the chains; consequently, most SMPs are glassy or semicrystalline polymer networks that have high stiffness at their application temperature. Nevertheless, applications are envisioned for soft (elastomeric) SMPs, including functionality enhancements for sealants, stamps, elastomers, and soft coatings. Despite the apparent need for soft SMPs,[4] only a few reports of soft shape memory polymers have appeared, including hydrogels with crystallizable alkyl side chains,[5] EPDM (ethylene propylene diene monomer) ionomers incorporating a range of crystallizable fatty acid salts,[6] a physical blend of a semicrystalline polymer and an elastomer,[7] and a semicrystalline nonwoven microfiber mat interpenetrated with a commercially available silicone elastomer[8] that was recently reported by our group. The present report describes an alternative approach to achieve soft SMP behavior, involving liquid crystallinity.

Liquid crystalline elastomers (LCEs) are soft thermosets whose network chains are comprised of alternating flexible segments and rigid mesogens. Architecturally, the elastomers may be of the side-chain type, where the mesogens are attached as pendent groups to the elastomeric network, or of the main-chain type, where the mesogens are incorporated into the backbone of the network chains. Interestingly, the level of orientational ordering intrinsic to LCEs is coupled to macroscopic strain, with order-reduction on heating leading to sample tensile contraction, a phenomenon pioneered by Finkelmann and co-workers[9,10] and described in numerous reviews[11–13] and a monograph.[14] Main-chain LCEs (MC-LCEs) offer a potential advantage over their side-chain counterparts due to anticipated stronger coupling of liquid crystalline order to macroscopic network deformation.[15] In the context of SMPs, LCEs show characteristic two-way, reversible, shape memory,[16–18] which is the reversible extension and contraction of the LCE when cooled and heated, respectively, through a first-order isotropization (nematic–isotropic or smectic–isotropic) transition under little to no applied static stress. This type of actuation—distinct from shape memory described above—abounds in the LCE literature, and authors have explained this elongation by the network's soft elasticity[18] and by the balance between the nematic field and the entropy of the network's chains.[19,20] A similar effect has also been reported around the crystallization and melting transitions in a non-liquid crystalline system based on chemically crosslinked polycyclooctene.[21]

In addition to reversible actuation properties of LCEs, our group has previously briefly reported one-way shape memory in a main-chain smectic-C liquid crystalline elastomer.[22] The ability of the MC-LCE to indefinitely fix a temporary shape and later remember and recover a permanent shape above room temperature is unexpected, considering these networks are based on poly(dimethylsiloxane) and remarkably soft. Here, we expand on that prior work by reporting on a series of main-chain LCEs based on a slender mesogen, ***5H***, copolymerized with a bulky co-mesogen, ***5tB***. Recognizing that ***5H*** tends to form liquid crystalline phases that are stable to higher temperatures than those containing ***5tB***, we are able to systematically vary the smectic–isotropic transition temperature of the LCE by diluting ***5H*** with ***5tB***. Bulk shape memory properties of the co-elastomers are reported, and a detailed investigation of the kinetics of recovery from the fixed state for one composition is shown. Finally, we demonstrate shape memory localized at the LCE's surface, a process that we envision will allow these materials to be employed as soft, active substrates for use in the microcontact printing and soft lithography fields.

Experimental

Main-chain liquid crystalline elastomers were prepared by reacting divinyl mesogens and a tetravinyl crosslinker with hydride end-capped poly(dimethylsiloxane) oligomer. The diene mesogens ***5H*** and ***5tB*** were synthesized according to methods described in literature.[23] The synthesis of **E-*5H*$_{80}$*5tB*$_{20}$** is given as an example of the main-chain LCE synthesis, noting that the only difference among the LCEs presented in this paper is the molar ratio of ***5H*** to ***5tB***. The nomenclature used throughout this paper is as follows: **E-** denotes that the material is an elastomer, ***5H*$_{xx}$** means that the LCE was synthesized with a mesogen molar feed ratio of *xx*% ***5H***, and ***5tB*$_{yy}$** means that the LCE was synthesized with a mesogen molar feed ratio of *yy*% ***5tB***.

Synthesis of E-*5H*$_{80}$*5tB*$_{20}$

Into a 25 mL flame dried and inert gas cooled Airfree™ reaction tube containing a magnetic stir bar, 0.205 mmol (99.8 mg) ***5H*** and 0.0514 mmol (27.8 mg) ***5tB*** were weighed. The solids were purged with nitrogen gas for 30 min, after which 0.41 mL of dichloromethane (purchased from Fisher Scientific and distilled over CaH_2 for dryness) was added to dissolve the solids at room temperature. The reaction tube was cooled to 0 °C before adding 12.5 μL (0.0257 mmol) of the crosslinker, tetrakis(vinyldimethylsiloxy)silane (Gelest), and 6 μL of Pt(0) catalyst (platinum(0)-1,3-divinyl-1,1,3,3-tetramethyldisiloxane complex in xylenes (Aldrich)). Next, 216 μL (0.308 mmol) dihydride-terminated poly(dimethylsiloxane), M_n 652 g mol^{-1} (^{1}H-NMR) (Aldrich), was added to the reaction, which was stirred to a homogeneous state. Expedient transfer to a sealed beaker coated with a hexamethyldisilazane hydrophobic release layer for polymerization and crosslinking in the desired film shape was required. For this, a 5 mL syringe and needle chilled over dry ice were used to transfer the reaction to a sealed 10 mL glass beaker that was equilibrated with dichloromethane atmosphere. The use of a chilled syringe and needle prevented gelation prior to transfer. The reaction was then allowed to proceed for 24 h at room temperature. After 24 h, the beaker was opened to reveal a MC-LCE film, which was easily removed from the glass floor of the beaker using tweezers. The elastomer was dried overnight in a fume hood before being dried further under vacuum at room temperature for 24 h. Once dried, the film was extracted four times using a mixed solvent consisting of equal parts by volume of dichloromethane and ethanol, and the film was once again dried at room temperature under vacuum. Gel fraction measurements were made in triplicate by weighing films before and after the extraction, dividing the post-extraction mass (m_{post})

by the pre-extraction mass m_{pre}, as indicated in eqn (1). On average all gel fractions exceeded 75%.

$$G(\%) = \frac{m_{post}}{m_{pre}} \times 100 \quad (1)$$

Characterization

All characterization experiments were performed on extracted elastomers that were relaxed by heating to 100 °C in a stress-free environment prior to testing. As will be shown, this temperature is well in excess of the isotropization temperature of the LCEs. The thermal transitions of the LCEs were studied using differential scanning calorimetry (DSC) and dynamic mechanical analysis (DMA), and the identification of the smectic phase was accomplished using wide-angle X-ray scattering. For all characterization experiments, the onset of mass loss (decomposition) determined by thermogravimetric analysis was found to exceed the maximum characterization temperature by at least 250 °C. For wide-angle X-ray scattering, film samples were mounted in the instrument (Rigaku S-MAX 3000 Pinhole SAXS system with adjustable sample-image plate distance) and exposed to Cu Kα radiation (1.54 Å) for 1 h. Two different sample-to-detector distances were required to study the reflections of the smectic layers, siloxane chains, and mesogens. For DSC, samples with mass of 2–4 mg were encapsulated in a TA Tzero standard aluminium pan and loaded into a TA Instruments Q200 Differential Scanning Calorimeter. The thermal program for these experiments was as follows: cool rapidly to $T = -90$ °C, hold isothermally for 1 min, heat at 10 °C min^{-1} to 100 °C ("first heat"), hold isothermally for 1 min, cool to $T = -90$ °C at 10 °C min^{-1}, hold isothermally for 1min, heat at 10 °C min^{-1} to 100 °C ("second heat"), hold isothermally for 1 min, and finally cool to −90 °C at 10 °C min^{-1} ("second cool"). The second heating and second cooling traces are presented, with heat flows normalized by sample mass.

Broad endothermic transitions observed during DSC heating runs were investigated in detail by an annealing study conducted using DSC. For these experiments, each LCE was heated rapidly to 100 °C and held isothermally for 10 min before cooling at 10 °C min^{-1} to a temperature, T_{anneal}, where the sample was held for 1 h. After the isothermal annealing, samples were cooled to −20 °C at 10 °C min^{-1}, held for 10 min, and finally heated at 10 °C min^{-1} to 100 °C. T_{anneal} values were selected to be approximately the temperature of the exotherm's maximum observed in the DSC "second cooling" trace (10 °C min^{-1}). Specifically, T_{anneal} was 45 °C for **E-*5H*$_{70}$*5tB*$_{30}$**, 50 °C for **E-*5H*$_{80}$*5tB*$_{20}$**, 55 °C for **E-*5H*$_{90}$*5tB*$_{10}$**, and 65 °C for **E-*5H*$_{100}$*5tB*$_{0}$**. The heating traces following the cooling–annealing–cooling sequence are reported, with heat flow normalized by sample mass.

Temperature-dependent linear viscoelastic properties for the LCEs were studied using a strain-controlled temperature ramp program in a TA Instruments Q800 Dynamic Mechanical Analyzer (DMA). Film samples were loaded initially under slight tensile load (amounting to 5–6 kPa) at room temperature to facilitate measurement of the sample length. This applied static load was maintained at 108% of dynamic load to maintain a state of tension in the sample even during tensile strain oscillation. The temperature dependence of linear viscoelastic properties was measured using a fixed oscillation frequency of 1 Hz and strain amplitude < 0.2% while heating at 3 °C min^{-1} from −70 °C to 150 °C. We report the tensile storage modulus, E', and loss tangent, tan(δ), values as functions of temperature.

The same Q-800 DMA was also used to characterize one-way shape memory behavior under a controlled force actuator mode. Samples were heated, stretched, cooled, unloaded, and heated again, all while monitoring the sample's tensile strain to reveal shape fixing and shape recovery completeness. For each experiment, a slender sample (typical dimensions: 5 mm × 1 mm × 0.4 mm) was first equilibrated at a temperature, T_{upper}, selected to be 15 °C above the maximum of the clearing point peak observed in the tan(δ) *versus* temperature trace from thermo-mechanical characterization described above. Next, the sample was loaded in the isotropic state to a stress of approximately 5 kPa, and the length of the specimen was recorded after 5 min of equilibration for use as the reference length in subsequent strain calculations. The shape memory "loop" begins with the deformation stage, wherein the sample is uniaxially stretched to a maximum stress of 100 kPa at a rate of 11.2 kPa min^{-1} and held isothermally for 5 min before the strain, ε_{def}, was recorded. Following the isothermal hold, the cooling stage was performed by decreasing the temperature at a rate of 2 °C min^{-1} to −40 °C (or other temperature). The sample was held isothermally for 5 min before the strain, ε_{cooled}, was recorded. The unloading stage then commenced, which consisted of a reduction in stress to 5 kPa at a rate of 11.2 kPa min^{-1} and an isothermal, constant force hold for 5 min. At this point the tensile strain, ε_{fixed}, was recorded. Finally, the cycle was completed with the recovery stage, where the sample was heated at a rate of 2 °C min^{-1} to T_{upper}, followed by an isothermal hold for 10 min, leading to the tensile strain, ε_{rec}. Two cycles were run consecutively for each of the composition, and two figures-of-merit measured: the degree of fixing (R_f) and the degree of recovery (R_r), calculated based on the equations shown below:

$$R_f(\%) = \frac{\varepsilon_{fixed}}{\varepsilon_{cooled}} \times 100 \quad (2)$$

$$R_r(\%) = \frac{\varepsilon_{cooled} - \varepsilon_{rec}}{\varepsilon_{cooled}} \times 100 \quad (3)$$

The kinetics of shape recovery were studied for a selected LCE, **E-*5H*$_{80}$*5tB*$_{20}$**, by stepwise heating of an initially strain-fixed sample with small temperature steps and prolonged strain-recovery measurements at each temperature. For these experiments, the sample was first equilibrated at 74 °C under a tensile stress of 5.6 kPa, and the length of the specimen after a 5 min equilibration established the reference length for subsequent strain calculations. This sample was then tested using the same shape memory protocol described above, with the only difference being during recovery stage. For these studies, the sample was heated to 30 °C at 2 °C min^{-1} and held isothermally at that temperature for 30 min. After this isothermal hold, the temperature was increased by 2 °C increments at a rate of 2 °C min^{-1} and then held isothermally at each incremental temperature for 30 min during which continued strain recovery occurred at a rate that depended on temperature. This experiment was repeated four times, and a typical plot of strain, stress, and temperature *versus* time will be reported. Additionally, the isothermal strain response to time was studied using regression analysis, the

parameters of which were averaged and reported with standard deviation.

The combination softness and shape memory of the studied LCEs offers the potential for reversible embossing of fine surface topography and this was tested for a selected sample, **E-*5H*$_{80}$*5tB*$_{20}$**. Thus, a shape memory cycle was localized at the surface of this sample through the use of contact-embossing with a patterned silicon wafer (master) prepared to feature square wells 30 μm in size at the surface and 10 μm in depth. For quantitative embossing, a TA Instruments AR-G2 Rheometer was employed, featuring highly parallel embossing plates with a 60 mm diameter circular top plate and opposing a larger diameter, bottom Peltier plate for cooling. The embossing master was placed on the bottom plate, with topographical features facing upward, and the LCE was stacked on top of the master before the top plate was placed in contact with LCE, though no normal stress was applied at this time. The sample was equilibrated at 74 °C for 5 min, following which the gap was decreased at a rate of 1 μm s^{-1}, leading to surface deformation of the LCE at the surface asperities of the master, continuing to a normal stress of approximately 200 kPa, a value low enough to avoid significant bulk deformation. The sample was then held isothermally for 5 min under this stress before cooling to 0 °C at 5 °C min^{-1}. Following a 5 min isothermal hold, the sample was unloaded by increasing the gap at a rate of 1 μm s^{-1} until no normal stress was measured. The LCE was then peeled from the wafer at 0 °C using tweezers, during which time the sample temperature rose to room temperature, or approximately 22 °C. Recovery of the embossed pattern to the permanent, flat, surface was accomplished by heating to 100 °C for 5 s in water. Topographical analysis of the embossing master, embossed LCE, and recovered LCE was accomplished using a KLA-Tencor P15 Surface Profiler with 300 μm × 300 μm scan area, 20 μm scan speed, 10 μm line spacing, and 65 μm height range with 0.0391 Å height resolution.

Results and discussion

5H-5tB LCEs with ***5H*** content varying between 70 and 100 mol% were synthesized as shown in Scheme 1 and as described in the Experimental section. The elastomers each form a smectic-C liquid crystalline phase, as shown by wide-angle X-ray scattering patterns obtained at room temperature (Fig. 1). Reflections due to periodic spacing of the smectic layers (Fig. 1c, $2\theta_{smectic}$ = 2.19–2.33°), backbones of the siloxane chains (Fig. 1b, $2\theta_{siloxane}$ = 12.0–12.2°), and the mesogens (Fig. 1b, $2\theta_{mesogen1}$ = 17.8–19.3° and $2\theta_{mesogen2}$ = 20.9–21.7°) are evident in Fig. 1 and are quite invariant with composition. The *d*-spacing values associated with each peak are reported in Table 1. Importantly, the *d*-spacings of the smectic reflections are significantly smaller than the computed for the extended repeating unit of 52.83 Å, suggesting a tilted smectic phase. Furthermore, our prior report[23] and supplementary X-ray data on stretched samples revealed splitting of the smectic ring into a four-point pattern consistent with a chevron-type arrangement of the smectic layers. The LCEs are thermotropic, and thus possess a smectic–isotropic transition temperature, hereafter referred to as an isotropization or clearing temperature. The temperature dependence of the phases was studied with DSC, where it was observed that the clearing temperature of the LCE decreases as ***5H*** loading is reduced (Fig. 1a). The endotherm and exotherm observed on heating and cooling, respectively, shift to lower temperatures as ***5H*** content is lowered in the LCE. Moreover, the transitions appear broader in

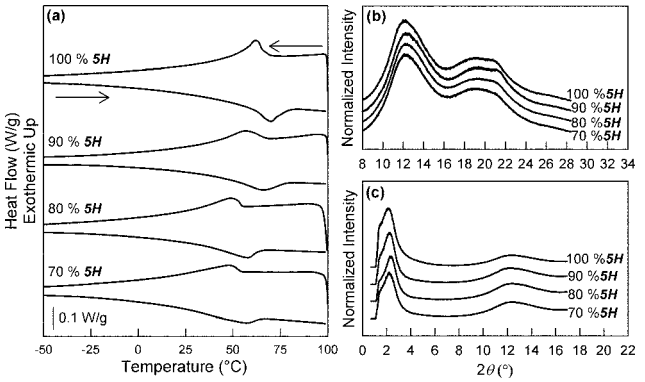

Fig. 1 Phase behavior of the ***5H-5tB*** LCEs. (a) DSC second heating and cooling traces at 10 °C min^{-1}. (b and c) Intensity *versus* 2θ from WAXS for sample-to-detector distances of: (b) 65.7 mm and (c) 236.4 mm.

Table 1 Summary of smectic layer, siloxane, and mesogen *d*-spacing from WAXS data

Material	$d_{smectic}$/Å	$d_{siloxane}$/Å	$d_{mesogen1}$/Å	$d_{mesogen2}$/Å
E-*5H*$_{100}$*5tB*$_0$	40.4	7.36	4.99	4.25
E-*5H*$_{90}$*5tB*$_{10}$	37.9	7.25	4.86	4.22
E-*5H*$_{80}$*5tB*$_{20}$	37.8	7.26	4.73	4.17
E-*5H*$_{70}$*5tB*$_{30}$	39.8	7.28	4.59	4.09

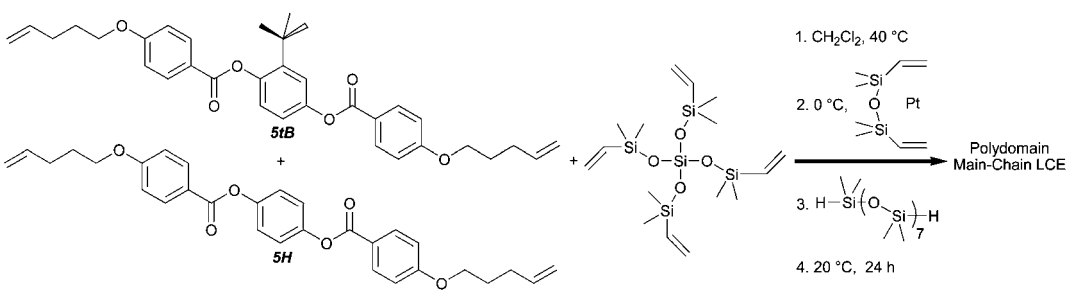

Scheme 1 Hydrosilylation synthesis of a polydomain main-chain liquid crystalline elastomer using the ***5H*** (R = H) and ***5tB*** (R = *tert*-butyl) mesogens. The mesogens and crosslinker were first dissolved in dichloromethane, then cooled to 0 °C where the Pt(0) catalyst and hydride-terminated poly(dimethylsiloxane) were added. This mixture was transferred to a crosslinking cell, where the reaction ran for 24 h.

the co-elastomers, with the broadness increasing as ***5H*** is replaced with ***5tB***. This apparent broadening is asymmetric—the low temperature side of the transition slopes into the heat flow signal—and we attribute this broadening to a second transition at a temperature lower than the clearing point. The presence of two transitions is more evident when the LCEs are studied with DSC after annealing for 1 h in the middle of the transition (Fig. 2) and when they are studied with DMA (Fig. 3), both described in more detail below.

Annealing the LCEs within the broad isotropization transition led to clear separation between an endothermic (isotropization) transition at higher temperatures and a stepwise change in the heat flow signal at lower temperatures (Fig. 2). This stepwise change in heat flow usually marks the glass transition temperature of a material, but our LCEs are not glassy below the transition, as revealed by their tensile storage modulus values that are all less than 100 MPa, even below the transition (Fig. 3). Thus, the midpoint of the heat flow step, marked by vertical lines in Fig. 2, is attributed to the glass transition (T_g) of the mesogens within the smectic layers, in a manner analogous to separate glass transitions for each phase reported in microphase-separated block copolymers, such as styrene–isobutylene–styrene.[24] Both the glass transition and the isotropization transition are composition-dependent and decrease as ***5H*** is replaced with ***5tB*** in the copolymer networks, as summarized in Table 2.

The temperature-dependent linear viscoelastic properties of LCEs are shown in Fig. 3. These samples were relaxed in the isotropic state, but not subjected to the annealing process described above. Each LCE shows a step-down in tensile storage modulus as the material is heated through the broad isotropization transition described above. Above this transition, the modulus of the LCE is similar to an isotropic rubber, is dominated by the crosslink density of the material, and hence is not strongly composition-dependent. At temperatures below this step, the modulus is two orders of magnitude higher than the isotropic modulus, but is almost two full orders of magnitude less than expected for a glassy polymer (~1 GPa). Closer analysis of **E-*5H*$_{100}$*5tB*$_0$** trace shows that the dramatic drop in storage modulus around 70 °C does not occur in one continuous step: there is a low temperature section with a smaller slope and a higher temperature section with a larger slope. The loss tangent trace for the same material supports this observation: a broad shoulder exists that is not fully separated from the more intense higher temperature peak. As the ***5H*** content is reduced, both the peak and shoulder observed in the loss tangent trace shift to lower temperatures, with the higher temperature peak moving to lower temperatures more quickly than the low temperature shoulder, resulting in the merging of the peaks for **E-*5H*$_{70}$*5tB*$_{30}$**. The decrease in the clearing temperature and the merging of the transitions as ***5H*** is replaced with ***5tB*** are thought to be due to the tendency of the ***5tB*** to vitrify rather than crystallize. A previous study[23] of the phase behavior of ***5H*** and ***5tB*** monomers showed that, in the monomer form, molten ***5H*** monomer will first form a nematic phase before crystallizing, and both melting and clearing endotherms are observed upon heating. In contrast, monomeric ***5tB*** cooled from the melt forms a nematic phase but will not crystallize unless it is annealed isothermally for an extensive period of time below the clearing transition. The ***5tB*** monomer instead tends to vitrify, as shown by a glass transition

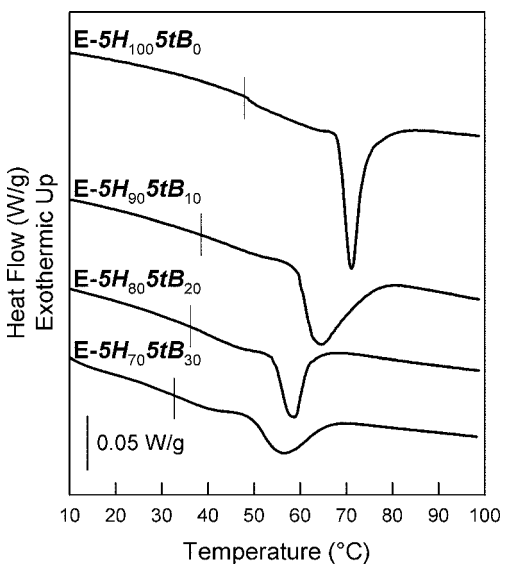

Fig. 2 DSC first heating traces after annealing. Samples were cooled from 100 °C at 10 °C min^{-1} to the annealing temperature (45 °C for **E-*5H*$_{70}$*5tB*$_{30}$**, 50 °C for **E-*5H*$_{80}$*5tB*$_{20}$**, 55 °C for **E-*5H*$_{90}$*5tB*$_{10}$**, and 65 °C for **E-*5H*$_{100}$*5tB*$_0$**), held isothermally for 1 h, and then cooled to −20 °C before heating at 10 °C min^{-1} to give the traces shown. Vertical lines mark T_g.

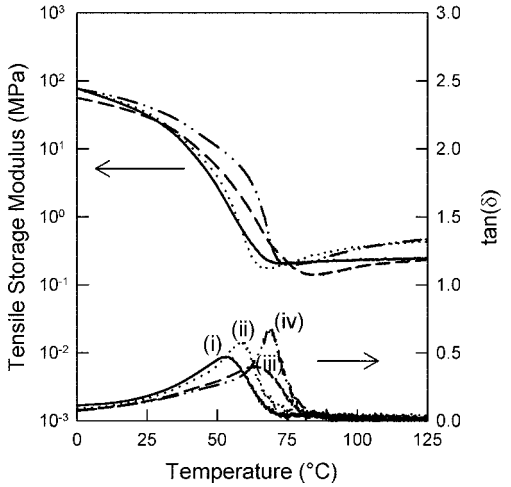

Fig. 3 Tensile storage modulus (E') and loss tangent (tan(δ)) traces of ***5H-5tB*** LCEs. Samples were relaxed in a stress-free state at 100 °C prior to testing (3 °C min^{-1} heating rate, 10 μm amplitude, 1 Hz frequency, 108% force track). Materials are identified by number and line style: **E-*5H*$_{70}$*5tB*$_{30}$** ((i), solid), **E-*5H*$_{80}$*5tB*$_{20}$** ((ii), dotted), **E-*5H*$_{90}$*5tB*$_{10}$** ((iii), dashed), and **E-*5H*$_{100}$*5tB*$_0$** ((iv), dashed-dot-dot).

Table 2 Summary of the glass transition (T_g) and isotropization (T_i) temperatures from the annealing DSC experiments shown in Fig. 2

Material	T_g/°C	T_i/°C
E-*5H*$_{100}$*5tB*$_0$	47.8	71.1
E-*5H*$_{90}$*5tB*$_{10}$	38.7	64.4
E-*5H*$_{80}$*5tB*$_{20}$	36.1	58.6
E-*5H*$_{70}$*5tB*$_{30}$	32.8	56.5

that is followed by a clearing endotherm when heated. In addition to its tendency to vitrify, ***5tB*** monomer also has a lower clearing temperature and latent heat of clearing, indicating that it forms a less stable liquid crystalline phase, which is likely due to the bulky *tert*-butyl substituent. The same behavior is expected for the LCE, where the bulky *tert*-butyl substituent disrupts the packing of the mesogens and causes the clearing temperature to decrease as ***5tB*** replaces ***5H***.

The high temperature peak in the loss tangent trace is correlated with the endotherm observed in the heating trace of the LCEs from the DSC and marks the isotropization transition of the LCE. Below this transition, the mesogens are organized in a smectic phase, but upon passing through this transition, the mesogens mix with the siloxane spacers, resulting in a detectable endothermic transition and the formation of an isotropic phase. The low temperature shoulder in the loss tangent trace tracks well with the step in heat flow observed calorimetrically and, while this suggests a glass transition, the modulus below the transition is two orders of magnitude less than a typical glassy material. Furthermore, these materials are at least 60 wt% siloxane and poly(dimethylsiloxane) is well above its T_g (−125 °C) at all temperatures studied. Considering the DSC and DMA data together, we attribute this transition to a glass transition of the mesogens within their smectic layers. The smectic layers may be thought of as a phase-separated block copolymer, where the siloxane chains and mesogens form two different blocks. In this case, the siloxane chains would allow the fluidity of the network to be maintained at the temperatures shown, but the phase-separated mesogens could independently vitrify within their layers if cooled sufficiently.

In the materials shown, the glass and clearing transitions are merged or nearly merged and are above room temperature, which we now show allows shape memory fixing and recovery of the soft networks temperatures gratifyingly close to (but above) room temperature. (While it is true that most crosslinked rubbers can be used as class I shape memory materials, their triggering temperatures are far too low for practical applications.) Shown in Fig. 4 are two one-way shape memory cycles of **E-*5H*$_{80}$*5tB*$_{20}$**. In both experiments, the LCE is deformed above the merged transition, cooled through both transitions under load to either −40 °C or 0 °C, unloaded, and then heated for recovery. Both cycles shown are representative of the excellent shape memory properties that are typical of these LCEs, despite the fact that they maintain a low modulus throughout the cycle (Fig. 3). While each composition was studied using the cycle cooled to −40 °C to be well below the merged transitions, the 0 °C cycle is reported to indicate that no improvement in shape memory fixing could be obtained by cooling to lower temperatures. The quality of shape memory fixing and recovery shown qualitatively in Fig. 4 is quantified in Table 3. The fixing ratios are always greater than 99% and do not improve with successive cycles, unlike the recovery ratios that improve to greater than 98% for all elastomers after one cycle. The higher recovery ratios observed in the second cycle may be due to the elimination of smectic layer defects after one cycle, as studies of lamellar block copolymers[25,26] and smectic systems[27] have been shown to have increased alignment and decreased number of defects when sheared at large amplitudes for increasing lengths of time. The reduction in defects in these studies was observed in the shear storage modulus and was found to be stable for at least a day after shear cessation. In this paper, the samples are deformed to large tensile strains, and we propose that this coarsening (defect elimination) is possible in our systems. However, we have no direct proof of this, or its causative role in yielding higher recovery ratios.

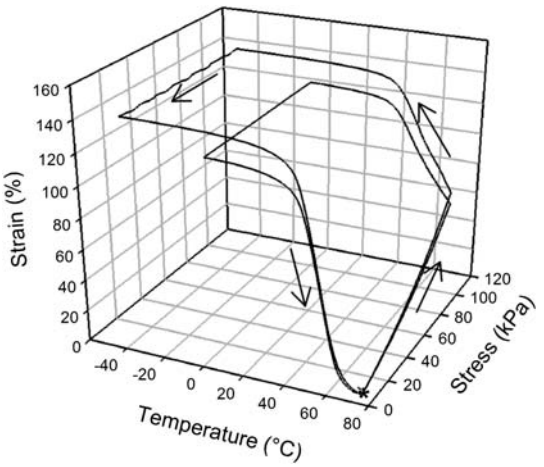

Fig. 4 One-way shape memory cycle of **E-*5H*$_{80}$*5tB*$_{20}$** deformed to a stress of 100 kPa at 74 °C, cooled under load to −40 °C and 0 °C, unloaded, and then heated to 74 °C for recovery. Shown for each experiment is the second cycle, where the beginning and end of the cycle are marked by the asterisk.

Table 3 Fixing ratio (R_f), recovery ratio (R_r), and actuation strain from the shape memory cycles of the ***5H-5tB*** LCEs. The temperatures at which 50% (T_{50}) and 90% (T_{90}) of the fixed strain is recovered are also shown

Material	Cycle	R_f (%)	R_r (%)	Actuation (%)	T_{50}/°C	T_{90}/(°C)
E-*5H*$_{100}$*5tB*$_0$	1	99.6	95.7	61.1	60.8	70.6
	2	99.6	99.2	54.8	61.8	74.1
E-*5H*$_{90}$*5tB*$_{10}$	1	99.5	92.2	51.3	62.6	73.6
	2	99.5	98.5	43.4	65.7	79.2
E-*5H*$_{80}$*5tB*$_{20}$	1	99.7	95.0	91.8	52.8	63.4
	2	99.7	98.1	73.4	54.9	68.1
E-*5H*$_{70}$*5tB*$_{30}$	1	99.6	96.7	105	44.7	60.2
	2	99.6	99.0	92.6	46.9	63.0

Because the elastomers under study are liquid crystalline, they elongate when cooled from the isotropic to the smectic phase under load, as reported by numerous other researchers.[28–30] This elongation on cooling is shown in Fig. 4 for the **E-*5H*$_{80}$*5tB*$_{20}$** cooled under 100 kPa of applied tensile stress. Interestingly, decreasing the applied tensile stress values resulted in a reduction of the temperature-onset for elongation, suggesting that the transition temperature increases with increasing stress. This observation is shown in Fig. 5 for **E-*5H*$_{80}$*5tB*$_{20}$**. The actuation strain (defined by eqn (4)) is the increase in the sample length between the end of the deformation stage and the end of the cooling stage in the one-way shape memory cycle. The actuation stain is reported in Table 3, but it is important to note that elongation started immediately on cooling the sample under this stress. In this sense, we expect that initiating the shape memory cycle at a higher temperature would reveal more (or all) of the actuation behavior and thus increase the measured actuation strain.

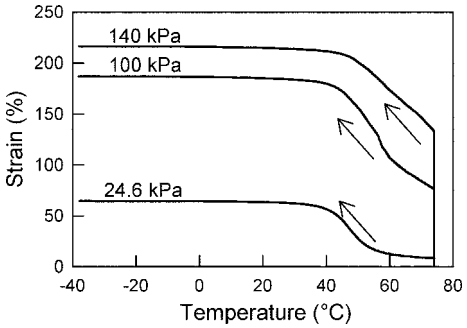

Fig. 5 Strain of **E-*5H*$_{80}$*5tB*$_{20}$** cooled at 2 °C min^{-1} under different tensile stresses (24.6 kPa, 100 kPa, and 140 kPa) in the DMA.

$$\varepsilon_{\text{actuation}}(\%) = \varepsilon_{\text{cooled}} - \varepsilon_{\text{def}} \quad (4)$$

The temperatures at which 50% (T_{50}) and 90% (T_{90}) of the fixed strain is recovered increase with increasing ***5H*** composition and successive cycles (Table 3). T_{50} for each LCE is between T_g and T_i reported in Table 2, and T_{90} exceeds T_i for the elastomers. This suggests that, while heating through T_g allows recovery of some strain, heating through isotropization may be required for complete recovery. This is not surprising, as actuation strain is recovered upon heating through the isotropization transition. Nevertheless, this finding prompted a detailed analysis of isothermal strain recovery using a stepped isothermal experiment.

The ability of a soft material to fix and recover strain well prompted a detailed investigation of the microstructure evolved during shape memory fixing and recovery (manuscript in preparation). Here, we sought to understand the effect the mesogen's T_g and the LCE's T_i have on the recovery of a fixed **E-*5H*$_{80}$*5tB*$_{20}$**. To this end, the LCE was fixed and, instead of heating continuously for recovery, the sample was heated to a temperature and held isothermally for 30 min before increasing the temperature by two degrees and repeating the isothermal step. Fig. 6 shows a plot of strain, stress, and temperature *versus* time for one such staged isothermal recovery experiment. The LCE elongated to 80% strain under applied stress and this increases significantly to *ca.* 175% strain upon cooling under load due to the liquid crystalline ordering under load, as discussed above. During the incremental isothermal strain-recovery steps, the strain followed an exponential time dependence.

In particular, the recovery data were well fit with the expression shown in eqn (5), where the three parameters considered for the fits included a relaxation time constant, τ, an exponential prefactor, A, and the strain offset, ε_o.

$$\varepsilon = \varepsilon_0 + Ae^{-t/\tau} \quad (5)$$

The relaxation time constant, τ, describes how rapidly the LCE reaches a quasi-equilibrium strain at that temperature. For further analysis, the prefactor A was normalized by ε_o to yield A/ε_o, a dimensionless value that describes the fraction of strain recovered during each isothermal hold. For all temperatures studied, four experiments were run (in separate experiments) to find average values for A/ε_o and τ. Fig. 7a and b show plots of A/ε_o and τ *versus* temperature with error bars denoting standard deviation. For close comparison with phase transition behavior, the tensile tan(δ) trace from dynamic mechanical analysis at a slow heating rate (0.5 °C min^{-1}) of the same material is shown in Fig. 7c. Not surprisingly, the normalized prefactor (strain increment) is negligible through the mesogen T_g; however, above this temperature, A/ε_o was observed to increase with temperature, becoming largest as the LCE approaches its clearing transition.

The recovery relaxation time similarly showed a "two region" temperature dependence, with τ remaining relatively independent

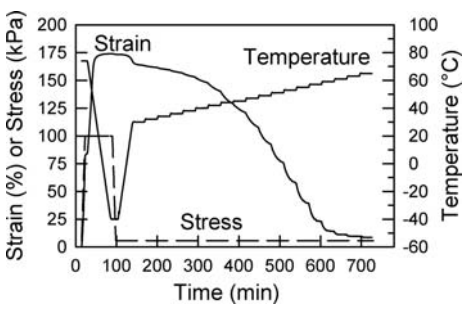

Fig. 6 Stepped isothermal recovery of **E-*5H*$_{80}$*5tB*$_{20}$**. The LCE was heated, deformed to a stress of 100 kPa, cooled (2 °C min^{-1}) under load, and unloaded to a stress of 5.6 kPa. The LCE was then heated at 30 °C and held isothermally for 30 min before increasing the temperature by 2 °C and repeating the isothermal step. Strain, stress, and temperature are plotted *versus* run time.

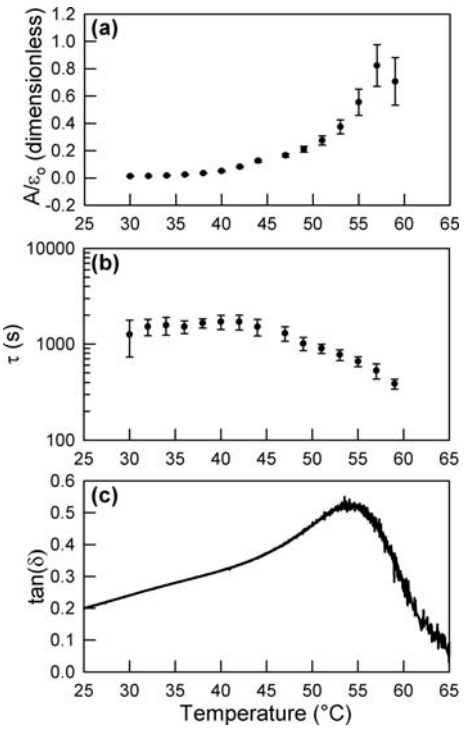

Fig. 7 Normalized prefactor (a) and relaxation time (b) *versus* recovery temperature for **E-*5H*$_{80}$*5tB*$_{20}$** and loss tangent trace (c) *versus* temperature from dynamic DMA trace (heating at 0.5 °C min^{-1}). Points in (a and b) are averages of four experiments and error bars denote standard deviation.

of temperature in the "glassy" state and then decreasing dramatically (notice the semi-log scaling in Fig. 7b) as the isothermal temperature approaches the clearing (isotropization) temperature. The decrease in relaxation time and increase in the normalized prefactor upon passing through T_g indicate the devitrification of mesogens releases the network chains to recover toward the equilibrium shape. The temperature dependence of τ was investigated for Arrhenius form by linear regression of a plot of log τ *versus* $1000/T$ (Fig. 8). This plot was found to be bi-linear, suggesting an Arrhenius dependence on temperature, though with two distinct activation energies. The linear regression fits are shown on the plot, and these curves have been extended to intersect the axes. At lower temperatures (or higher $1000/T$ values) the linear regression curve ($R^2 = 0.987$) yielded an activation energy of 71.2 kJ mol^{-1}. Closer to the isotropization temperature, the activation energy was measured to be a larger value, 138.7 kJ mol^{-1}; however, only two points were used for this fit, yielding an artificially high R^2 value of 1.0. Though not presented here,[31,32] the decrease in τ with increasing temperature occurs at temperatures where microstructural changes in the mesogen tilt angle and chevron pitch of the smectic layers have been observed using wide-angle X-ray scattering (see ESI†). Therefore, we postulate that the temperature-dependent LCE microstructure affects shape memory recovery by dictating the mobility of the mesogens and smectic layers.

An application of soft shape memory polymers is a shape memory cycle localized reversibly on the surface of a material, or "reversible embossing". Fig. 9 shows topographic (surface) images that are three-dimensional plots of the surface profile of the master (Fig. 9a), the embossed **E-*5H*$_{80}$*5tB*$_{20}$** LCE (Fig. 9b), and the recovered LCE (Fig. 9c). The master is a silicon wafer patterned topographically to consist of square wells (30 μm × 30 μm) that are separated by 30 μm. Both of these dimensions were measured at the surface of the master; it should be noted that the dimensions of the wells vary with depth and are 15 μm × 15 μm at their base. The initial state of the LCE is flat. When the LCE is embossed by application of pressure above the isotropization temperature ($T_i = 59$ °C), the elastomer is deformed into the wells of the master. This deformation is "frozen" on the still-soft surface upon cooling to 0 °C, presumably by the same mechanism as bulk strain fixing as described above; namely, mesogen vitrification. The result of this is the fixing of pillars on the surface of the LCE. Like bulk shape memory, the permanent shape, a flat topography in this case, can be recovered by heating the LCE above the isotropization temperature, in this case in 100 °C water. As shown in Fig. 9c, the recovery to flatness is quite complete.

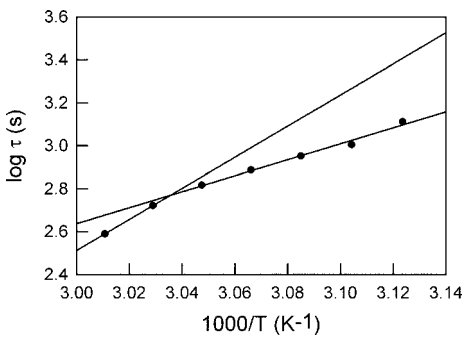

Fig. 8 Log of relaxation time *versus* recovery temperature for **E-*5H*$_{80}$*5tB*$_{20}$** with linear regression lines fit to the data and extended to the axes.

The surface topography of reversibly embossed **E-*5H*$_{80}$*5tB*$_{20}$** was studied quantitatively using profilometry, plotting the height, z, *versus* position on the surface (Fig. 9d). The profile for the master matches the geometry described above: wells with a base width of 15 μm and a height of 10 μm are spaced 30 μm apart (Fig. 9d, trace (i)). The embossed LCE trace (Fig. 9d, trace (ii)) shows that the pillars formed by embossing are not a perfect inverse of the wells in the master, however. Those pillars with a height equal to the depth of the wells in the master were found to have peaks larger in area than the base of the wells in the master. These pillars also were closer together than expected. Pillars not reaching the maximum height of the wells were found to obey the geometry of the master better: that is, they had peak areas and spacings that were very close to the inverse of the master. Furthermore, the sides of the pillars are curved, not straight like the master. These findings indicate that, while degree of fixing of the profile height can be quite high, the fidelity of the pattern is not always conserved. It is thought that the differences in dimensions and the curvature of the pillars are due to the storing of additional energy in the LCE. In this case, the film may have been not uniform in thickness, causing a gradient of applied stress. If the stress applied exceeded that required to press the LCE into the wells, the LCE would fix this excess energy upon cooling and this could be manifested by a dimensional change in the pattern. Interestingly, the recovered LCE shows a flat topography with no regular features (Fig. 9d, trace (iii)), indicating near-perfect shape recovery.

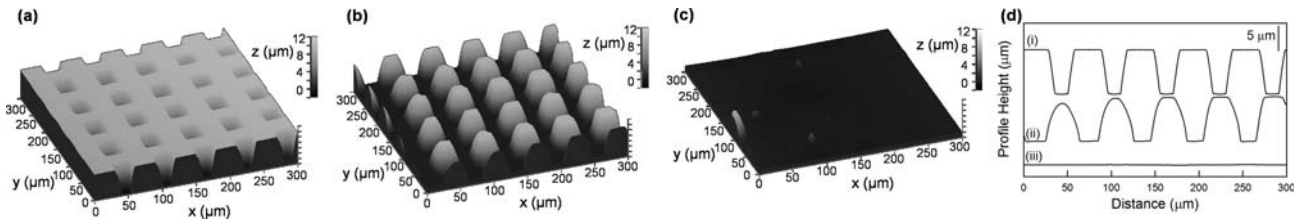

Fig. 9 Surface shape memory of **E-*5H*$_{80}$*5tB*$_{20}$**. 3D plots obtained from surface profilometry show the topography of the embossing master (a), LCE embossed with the master (b), and embossed LCE after it was recovered by heating in 100 °C water (c). Each scan shows a 300 μm × 300 μm area at the same z axis scale, −2 μm to 12 μm. The profile height *versus* distance along x axis at constant y position is shown in (d) for the embossing master (i), embossed LCE (ii), and recovered LCE (iii).

Like the bulk state, a crosslinked network is required during heating to preserve mechanical integrity while rubber elasticity drives recovery by increasing entropy of the chains. While, in principle, any physically or chemically crosslinked polymer network may be embossed reversibly, soft shape memory polymers require less stress input for the deformation while allowing "flow" into fine features of a mold. An envisioned application of these soft, active substrates is as a reversible, soft lithographic master, stamp, or microfluidic networks.

Conclusions

We have reported the synthesis and characterization of a range of main-chain LCEs with compositional variations that adjusted the transition temperatures of the smectic materials, including the glass transition temperature of the mesogen-rich layers and the isotropization temperature of the smectic phase. The shape memory behavior of the LCEs was characterized to reveal substantial strain fixing and recovery (each >98%), despite material softness above and below the shape memory critical temperature. Detailed kinetic analysis for shape recovery was reported for a selected composition, using a stepwise temperature ramp, revealing single exponential decays of strain with time and strong temperature dependence of the characteristic recovery times. The low modulus (softness) of the studied LCEs was exploited in the demonstration and quantification of reversible embossing wherein a photolithographed master embossed an LCE with good replication. The embossed pattern could be completely erased by heating.

Acknowledgements

The authors are grateful for the support of the National Science Foundation. PTM acknowledges support from National Science Foundation (DMR-0758631). KAB acknowledges the support of a Graduate Research Fellowship from the National Science Foundation (DGE-0234629).

References

1 A. Lendlein and S. Kelch, *Angew. Chem., Int. Ed.*, 2002, **41**, 2034–2057.
2 C. Liu, H. Qin and P. T. Mather, *J. Mater. Chem.*, 2007, **17**, 1543–1558.
3 P. T. Mather, X. Luo and I. A. Rousseau, *Annu. Rev. Mater. Res.*, 2009, **39**, 445–471.
4 P. T. Mather, *Nat. Mater.*, 2007, **6**, 93–94.
5 Y. Osada and A. Matsuda, *Nature*, 1995, **376**, 219.
6 R. A. Weiss, E. Izzo and S. Mandelbaum, *Macromolecules*, 2008, **41**, 2978–2980.
7 H. Zhang, H. T. Wang, W. Zhong and Q. G. Du, *Polymer*, 2009, **50**, 1596–1601.
8 X. Luo and P. T. Mather, *Macromolecules*, 2009, **42**, 7251–7253.
9 H. Wermter and H. Finkelmann, *e-Polymers*, 2001, **013**, 1–13.
10 K. Hiraoka and H. Finkelmann, *Jpn. J. Appl. Phys.*, 2009, **48**, 061505.
11 S. Krause, F. Zander, G. Bergmann, H. Brandt, H. Wertmer and H. Finkelmann, *C. R. Chim.*, 2009, **12**, 85–104.
12 P. Xie and R. B. Zhang, *J. Mater. Chem.*, 2005, **15**, 2529–2550.
13 K. Urayama, *Macromolecules*, 2007, **40**, 2277–2288.
14 M. Warner and E. M. Terentjev, *Liquid Crystal Elastomers*, Oxford University Press Inc., New York, 2003.
15 P.-G. de Gennes, *C. R. Acad. Sci., Ser. IIb: Mec., Phys., Chim., Astron.*, 1997, **324**, 343–348.
16 D. L. Thomsen, P. Keller, J. Naciri, R. Pink, H. Jeon, D. Shenoy and B. R. Ratna, *Macromolecules*, 2001, **34**, 5868–5875.
17 C. Ortiz, M. Wagner, N. Bhargava, C. K. Ober and E. J. Kramer, *Macromolecules*, 1998, **31**, 8531–8539.
18 A. R. Tajbakhsh and E. M. Terentjev, *Eur. Phys. J. E*, 2001, **6**, 181–188.
19 J. M. Adams and M. Warner, *Eur. Phys. J. E*, 2005, **16**, 97–107.
20 M. Tokita, H. Tagawa, H. Niwano, K. Osada and J. Watanabe, *Jpn. J. Appl. Phys.*, 2006, **45**, 1729–1733.
21 T. Chung, A. Romo-Uribe and P. T. Mather, *Macromolecules*, 2008, **41**, 184–192.
22 I. A. Rousseau and P. T. Mather, *J. Am. Chem. Soc.*, 2003, **125**, 15300–15301.
23 I. A. Rousseau, H. H. Qin and P. T. Mather, *Macromolecules*, 2005, **38**, 4103–4113.
24 R. F. Storey, B. J. Chisholm and M. A. Masse, *Polymer*, 1996, **37**, 2925–2938.
25 K. I. Winey, S. S. Patel, R. G. Larson and H. Watanabe, *Macromolecules*, 1993, **26**, 2542–2549.
26 K. I. Winey, S. S. Patel, R. G. Larson and H. Watanabe, *Macromolecules*, 1993, **26**, 4373–4375.
27 R. G. Larson, K. I. Winey, S. S. Patel, H. Watanabe and R. Bruinsma, *Rheol. Acta*, 1993, **32**, 245–253.
28 R. Ishige, K. Osada, H. Tagawa, H. Niwano, M. Tokita and J. Watanabe, *Macromolecules*, 2008, **41**, 7566–7570.
29 M. Bispo, D. Guillon, B. Donnio and H. Finkelmann, *Macromolecules*, 2008, **41**, 3098–3108.
30 P. Beyer, E. M. Terentjev and R. Zentel, *Macromol. Rapid Commun.*, 2007, **28**, 1485–1490.
31 K. A. Burke and P. T. Mather, in 2009 Materials Research Society Spring Meeting, San Francisco, California, 2009.
32 K. A. Burke and P. T. Mather, in 5th International Liquid Crystal Elastomer Conference, Kent, Ohio, 2009.